Eur. Phys. J. Spec. Top. (2026) 235:9139–9156
https://doi.org/10.1140/epjs/s11734-026-02569-4

THE EUROPEAN PHYSICAL JOURNAL SPECIAL TOPICS

Regular Article

Recurrence lacunarity of spatial data

Cara Bielig[1,2,a], Tobias Braun[1,3,b], Matheus S. Palmero[1,4,c], Aljoscha Rheinwalt[2,d], and Norbert Marwan[1,2,e]

[1] Complexity Science, Potsdam Institute for Climate Impact Research, Telegrafenberg A 31, 14473 Potsdam, Brandenburg, Germany
[2] Institute of Geosciences, University of Potsdam, Am Neuen Palais 10, 14469 Potsdam, Brandenburg, Germany
[3] Institute for Earth System Science and Remote Sensing, University Leipzig, Talstrasse 35, 04103 Leipzig, Saxonia, Germany
[4] Instituto de Ciências Matemáticas e de Computação, Universidade de São Paulo, 13560-970 São Carlos, SP, Brazil

Received 2 February 2026 / Accepted 31 July 2026 / Published online 9 October 2026
© The Author(s) 2026

Abstract Quantifying the structure and heterogeneity of complex spatial patterns remains a key challenge in spatial data analysis. Recurrence plots (RPs) offer a powerful method for visualizing the recurrent spatial patterns in such data. To quantify the structure of spatial recurrences, we extend the normalized recurrence lacunarity (nRL), a measure of the homogeneity of an RP, to the analysis of spatial RPs. Even though RPs can be derived from data with a topological dimension larger than one, their nRL has yet to be evaluated. To address this gap, we evaluate the nRL of spatial RPs, validate the method using synthetic test patterns and model data, and then apply it to analyze the hillslope gradients of 47 river catchments near the Mendocino Triple Junction. The results suggest that the nRL effectively detects and quantifies subtle differences in the spatial structure of the catchments. We show indications that these relate to local uplift rates, a previously identified possible driver of the structural differences. The nRL provides a robust and scale-sensitive tool for comparing diverse spatial data sets and for detecting and quantifying how their spatial structure may relate to external parameters.

1 Introduction

Since their introduction in 1987 by [1], recurrence plots (RPs) have become an established tool for the analysis of time series and phase-space trajectories of dynamical systems. Initially, the analysis of RPs was qualitative and based on their visual appearance, until Zbilut and Webber Jr. [2] introduced recurrence quantification analysis (RQA) with different quantitative measures. RQA measures quantify the texture of an RP based on the distribution of the lengths of diagonal and vertical lines that form within the RP [2, 3]. As an additional quantifier that does not depend on the existence of line structures, [4] introduced the lacunarity of RPs, a measure from fractal geometry, referring to it as the recurrence lacunarity (RL). Although the lacunarity measure was originally introduced by [5] to quantify how fractals fill space, this concept can be transferred to RPs, where the measure captures the variance of the mass distribution over an RP. In the context of RPs, the "mass" can be interpreted as a local recurrence rate (RR). Successful applications in geosciences include [6], who use the RL to quantify the diversity of the behavior of atmospheric regimes that they detected using a combination of kernel principal component analysis and recurrence analysis. [7] use the lacunarity to develop a lacunarity-based index for spatial heterogeneity, which they apply to binary and non-binary synthetic patterns and spatial sea ice coverage data. Furthermore, [8] applied the RL to detect subtle structural changes in financial data (stock indices) as well as to detect damages in train tracks by analyzing time series from axle box acceleration vibration data. In [9], the authors defined different approaches to capture fractal properties of time series, including an approach that resembles the RL strongly. They compare the approaches in terms of the quality of their results and their applicability using synthetic and empirical data from a

[a] e-mail: cara.bielig@uni-potsdam.de (corresponding author)
[b] e-mail: tobias.braun@uni-leipzig.de
[c] e-mail: palmero@usp.br
[d] e-mail: aljoscha.rheinwalt@uni-potsdam.de
[e] e-mail: marwan@pik-potsdam.de

study of human behavior and found the approach to be especially suitable for comparing the fractal dimensionality of persistent data.

Whereas previous applications included only two-dimensional RPs, the concept of RPs and RQA was extended to higher dimensions by [10]. They introduced the generalized RP together with the generalized RQA, enabling the analysis of image data. RL has only been used with traditional RPs, applying it to higher-dimensional RPs remains to be shown. In this paper, we take a first step in this direction by applying the RL as defined by [4] to four-dimensional (spatial) RPs derived from spatial data.

RPs provide a standardized transformation of various kinds of data into a binary pattern, enabling direct comparability across data sets irrespective of absolute value ranges. Furthermore, spatial RPs capture directional information that complements static image analysis. This makes the RL applicable to any type of spatial data, including higher-dimensional spatial data (such as multi-channel data), as long as it can be converted to an RP. It quantifies the structure of spatial data on different scales and can detect (the scale of) recurring sub-patterns, outliers, and noise. In this context, the RL could help reveal subtle, less obvious characteristics of the data, e.g., pattern transitions or small-scale perturbations related to noise. The RL complements standard statistical measures by capturing spatial structure across scales. It can identify and quantify links between spatial structure and external factors and could be applied in classification or machine-learning workflows.

In this paper, RPs will shortly be introduced in Subsect. 2.1, followed by their extension to spatial data in Subsect. 2.2. Then, the normalized recurrence lacunarity (nRL) is introduced in Sect. 2.3 following the definition of [4] and subsequently extended to spatial RPs. In Sect. 3, the nRL is applied to synthetic patterns that highlight key properties of the measure, before applying the nRL to model data from a rock-paper-scissors (RPS) system in Sect. 4 as a bridge between synthetic data and empirical data. Finally, the method is applied to the hillslope gradients of 47 small coastal river catchments along the coast of California in Sect. 5 as an example of a real-world use case. Sections 6 and 7 discuss and summarize the findings, respectively.

2 Methodology

2.1 Recurrence plots

RPs were first introduced with the purpose of visualizing the behavior of phase-space trajectories [1]. They are a tool for understanding the typical properties of a system and predicting its future behavior [11]. RPs can be obtained from individual time series or from phase-space trajectories. If no trajectory is available for a system, it can often be reconstructed from a single time series, e.g., using time-delay embedding [12].

RPs visualize the recurrences of a system's state $\vec{a}_i$ in a phase space within a small deviation ε [1, 11]. A RP consists of a two-dimensional binary matrix $\mathbf{R}$,

$$R_{i,j} = \Theta(\varepsilon - \|\vec{a}_i - \vec{a}_j\|), \qquad \vec{a}_i \in \mathbb{R}^m, \qquad i, j = 1, \ldots, N, \tag{1}$$

where recurrences are represented by the value 1 (usually black dots). $\Theta(\cdot)$ denotes the Heaviside function, $\|\cdot\|$ represents a suitable norm (here: Euclidean norm), ε is the recurrence threshold, $\|\vec{a}_i - \vec{a}_j\|$ is the spatial difference between two different states of the system at times i and j and m is the dimension of the phase space [11]. The two axes in the RP represent time.

In this work, the distance threshold ε is kept constant for each pair of $\vec{a}_i$ and $\vec{a}_j$. For continuous data, by choosing ε as a certain percentile of the distances between all $\vec{a}_i$ and $\vec{a}_j$, the ratio of recurrences to all pixels in the RPs can be controlled. This ratio is referred to as the recurrence rate (RR) and ensures the comparability of different RPs [13]. For discrete data, where data values represent distinct categories and numerical proximity does not imply state similarity, $\varepsilon = 0$. This ensures that only the recurrence of the exact same state is reflected in the recurrence plot.

Depending on the properties of the studied system, diagonal, vertical, and horizontal lines of various lengths form in the RP. Based on the number and length of these structures, the texture of an RP can be quantified [2, 3]. Measures based on the line length distributions of vertical, horizontal, and diagonal lines form the basis for recurrence quantification analysis (RQA) [11].

2.2 Spatial recurrence plots

Equation 1 can be extended to higher dimensions [10]:

$$R_{\vec{i},\vec{j}} = \Theta\left(\varepsilon - \left\|\vec{a}_{\vec{i}} - \vec{a}_{\vec{j}}\right\|\right), \qquad \vec{a}_{\vec{i}} \in \mathbb{R}^m, \qquad \vec{i}, \vec{j} \in \mathbb{N}^d, \tag{2}$$

Table 1 Interpretation of the two-dimensional axis-parallel subsets of the RP

x_1	y_1	x_2	y_2	Interpretation
fixed	fixed			Comparison of the whole image to one image pixel
fixed		fixed		Comparison of two image rows
fixed			fixed	Comparison of one image column and one image row
	fixed	fixed		Comparison of one image row and one image column
	fixed		fixed	Comparison of two image rows
		fixed	fixed	Comparison of the whole image to one image pixel

providing the RP for a d-dimensional system (topological dimension, not the dimension of the phase space). In contrast to Eq. 1, where a system state is represented by a single coordinate i, there is now a d-dimensional coordinate vector $\vec{i}$ [10]. For two-dimensional data (spatial data), the coordinate vector consists of the two image pixel coordinates x_i and y_i, finally resulting in a four-dimensional recurrence matrix. In a four-dimensional (spatial) RP, the recurrences can form vertical, horizontal, and diagonal one- or higher-dimensional structures in various directions. From the number and sizes of these structures, the measures of the generalized recurrence quantification analysis (GRQA), which is the extension of the RQA to higher dimensions, can be derived [10].

In Figs. 1 and 2, four exemplary patterns are displayed, together with two-dimensional subsets of their respective spatial RPs. In this visualization of the RPs, the horizontal plane visualizes the RP of one image row (here: center row, $y_1 = y_2 = 50$), while the vertical plane displays the similarity between one image pixel (here: the center pixel of the rightmost column, $x_2 = 99$ and $y_2 = 50$) and the whole image.

The two-dimensional subsets highlight the additional information of the RP transfers about the underlying pattern. In total, six different two-dimensional subsets that are parallel to the axes of the RP can be extracted. Whereas two of the possible subsets, where one image pixel is compared to the whole image, reproduce the underlying image, the other subsets offer information about changes in specific directions and have the potential to reveal directional anisotropies. Table 1 gives an overview of the interpretation of the different subsets. Next to these axis-parallel subsets, various other two-dimensional subsets can be extracted from the RP, whose interpretation is more challenging.

2.3 Recurrence lacunarity

The measure of lacunarity has recently been proposed as recurrence lacunarity (RL) to quantify the homogeneity of an RP [4]. Here, the RL of spatial RPs is evaluated. Building on the work of [4], the same RL definition is applied.

In contrast to the measures included in the RQA or GRQA, the RL is not based on the distribution of line lengths, but on the distribution of masses of boxes of varying sizes within the RP [4].

For the computation of the RL for a specific box size w, a grid with boxes of size w is placed over the RP. The mass of each box is defined as the sum of recurrences within each box. The first and second moments of the distribution of the masses at a box size w form the basis for the computation of the RL. The moments of the mass distribution are calculated by [4]

$$Z^{(q)}(w) = \sum_{M} M^q p_w(M), \tag{3}$$

where $p_w(M)$ represents the relative frequency of the mass M at a box size w.

The RL $\Lambda(w)$ for a specific box size w is calculated by dividing the second moment by the square of the first moment,

$$\Lambda(w) = \frac{Z^{(2)}(w)}{\left[Z^{(1)}(w)\right]^2}. \tag{4}$$

In other words, the RL is the ratio of the mean squared mass to the square of the mean mass. The RL equals 1 if all the recurrences in the RP are equally distributed among the individual boxes (indicating a *homogeneous* RP) and increases if the recurrences are less equally distributed among the boxes (indicating a more *heterogeneous* RP).

To normalize the RL, the RL of the inverted RP $\bar{\Lambda}(w)$, where all 1 s are exchanged with 0 s and *vice versa*, is also considered. This has the advantage that not only the distribution of 1 s in the RP is analyzed, but the

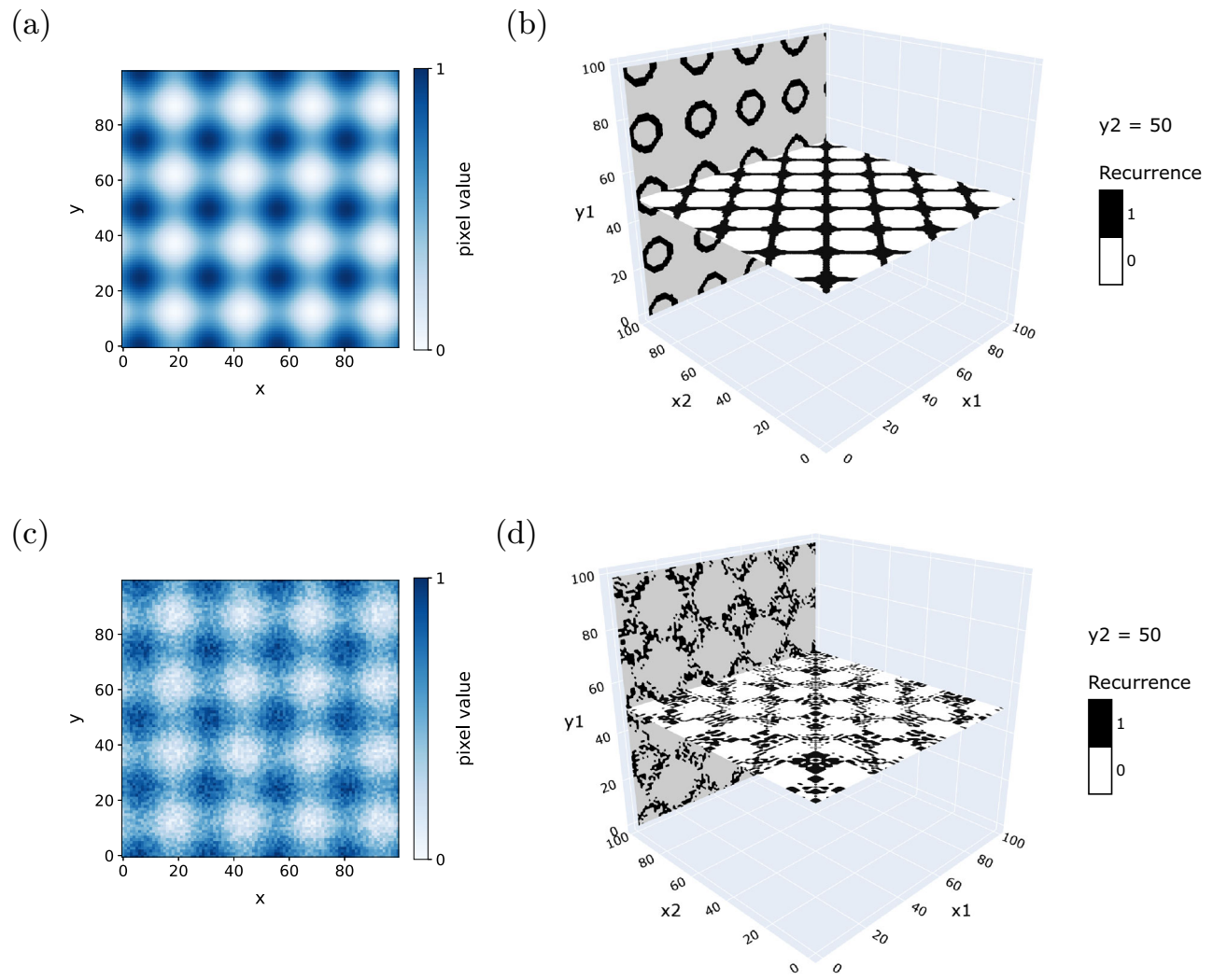

Fig. 1 Synthetic periodic patterns with two-dimensional subsets of their respective spatial RPs. **a**, **b** periodic pattern, $RR \approx 20\%$; **c**, **d** periodic pattern with random white noise, $RR \approx 20\%$

distribution of 0 s is also accounted for. The normalized recurrence lacunarity (nRL),

$$\Lambda^*(w) = 2 - \left(\frac{1}{\Lambda(w)} + \frac{1}{\bar{\Lambda}(w)} \right), \tag{5}$$

approaches 0 if all recurrences are equally distributed between all boxes, indicating again that the RP is *homogeneous* on this scale. It approaches 1 if all recurrences are concentrated within a subset of boxes, whereas other boxes remain empty, indicating that the RP is *heterogeneous* on this scale [4].

It is important to note that this normalized formulation differs fundamentally from the classical lacunarity: whereas the standard lacunarity decreases monotonically and converges to unity at large scales, the nRL is bounded between 0 and 1 by construction [14]. Although local minima and maxima can appear in standard lacunarity curves, the normalization amplifies these features, rendering characteristic length scales of the underlying spatial pattern more clearly detectable [15].

For a time series or phase-space trajectory, a box within the RP equals the sampling of two segments from the data, and comparing the segments in terms of their recurrences (similarity defined by the recurrence threshold ε) [4]. The number of recurrences between the two segments defines the mass of the box. If all segment pairs contain a similar number of recurrences, the nRL is closer to 0. If some segment pairs contain many similar values, whereas other segment pairs differ a lot, the nRL is closer to 1. Consequently, on each scale w, the nRL quantifies the deviation of the masses from translational invariance [4]. This property enables the detection of transitions between different dynamical states of a system and their respective temporal scales, indicated by sudden changes

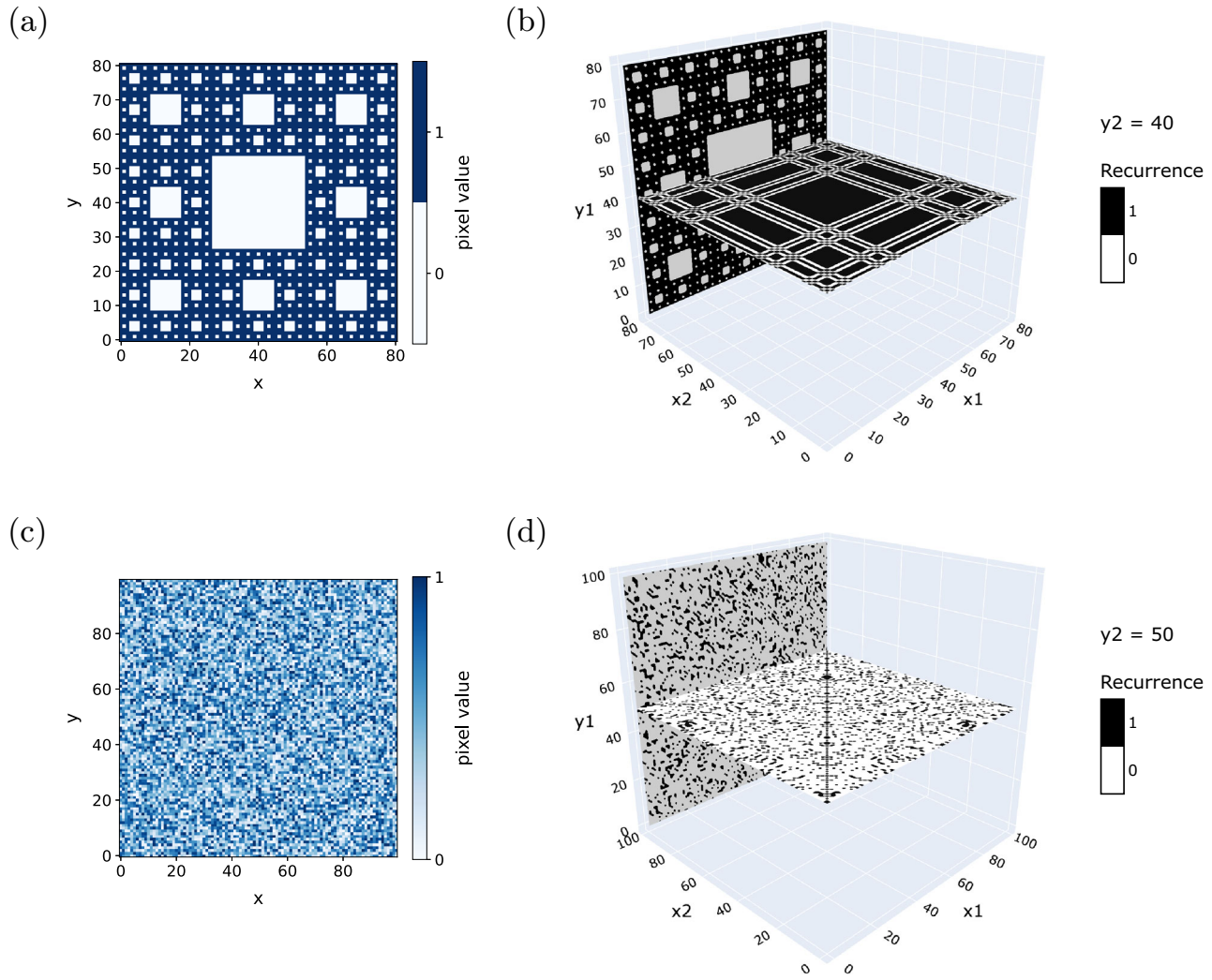

Fig. 2 Synthetic patterns with two-dimensional subsets of their respective spatial RPs. **a**, **b** Sierpiński carpet, $\varepsilon = 0$; **c**, **d** uniformly distributed white noise, $RR \approx 20\%$

in the nRL values. Power-law behavior is inherent to Recurrence Lacunarity (RL). Deviations from this power law, local maxima and minima, indicate the presence of characteristic scales within the system.

For spatial data, the computation of the nRL follows the same steps as for one-dimensional data (topological dimension), with the difference that the boxes in the spatial RP are not two-dimensional, but four-dimensional. The mass of a box in a spatial RP represents the number of recurrences between two square patches within the image. The nRL captures the distribution of the masses and, therefore, quantifies the heterogeneity of the RP, not of the underlying data. Therefore, the nRL reflects the reuse of local spatial configurations (sub-patterns), providing access to pattern-level correlations that cannot be assessed through the lacunarity of the image, which is purely geometrical and does not consider how configurations may organize anisotropically. Structural properties of the underlying data can be inferred from three primary features of the nRL curve (calculated using non-overlapping boxes): its local minima, local maxima, and the shape of the curve.

Minima appear when the nRL is especially low for a certain box size w. For this scale, the recurrences are relatively equally distributed among the boxes (which also applies to the inverse RP), meaning the RP appears *homogeneous* on this scale. This suggests recurring sub-patterns or the systematic absence of such sub-patterns in the data that are linked to this scale.

Maxima appear when the RP is especially *heterogeneous* on a certain scale, meaning the recurrences are accumulated within a subset of boxes, and the remaining boxes are sparsely filled. While accumulations of recurrences could originate from self-similar recurring sub-patterns (values within the square image patches are similar within

themselves and compared to the other patch), gaps in the RP can appear due to outliers or spatial regime shifts, which both mark image regions that lack recurrences in the remainder of the image.

While minima and maxima are deviations from the typical power law behavior and highlight characteristic length scales within the data, the shape of the nRL curve reflects how the RP appears on all different scales w. The power law exponent of the nRL curve reflects how fast heterogeneity in the RP disappears as one zooms out/coarse-grains the RP. Large exponents indicate that a system recurs irregularly at short times, but recurs more uniformly when coarse-grained. Small values suggest more complex recurrence across all scales. A later cut-off of the power law implies strong heterogeneity in the RP persisting on larger scales, indicating larger accumulations of recurrences or gaps in the RP. The cut-off of the curve can, therefore, be used to estimate the scale beyond which the RP becomes approximately translationally invariant. This scale, again, marks an important length scale within the data by indicating where smaller-scale spatial variations fade into large-scale homogeneity.

Compared to applying lacunarity directly to the original image using standard binarization, the RP-based approach offers distinct advantages. First, lacunarity works better for binary images and would, therefore, require a binarization of the original image for this use case. Such thresholding of the original image can strongly influence the result by discarding continuous intensity information; the RP-based approach instead encodes the full continuous distance structure of the data first and then applies the recurrence threshold on these distances, thus including information about the entire range of intensity values. Second, since the RP is constructed from pairwise comparisons of local states, the approach generalizes naturally to multivariate or multi-channel spatial data (vector data), where the standard lacunarity approach is not defined for vector data. Third, because the dimensions of the RP capture directional pairwise relationships, the nRL is sensitive to anisotropic organization of spatial configurations—structural differences that depend on orientation—which a lacunarity computed directly on an image cannot detect, as it treats the image geometry independently of how sub-patterns occur across directions.

The higher computational cost of the spatial RP construction relative to direct image lacunarity is a practical limitation for very large images, but it is the price of the additional information content that the RP encodes.

To compute the nRL curve, a grid of non-overlapping boxes of size w is placed over the RP, anchored at the upper-left corner (i.e., (0,0,0,0) in the four-dimensional RP). The mass in each box is then computed and used to derive the nRL for each w. For large four-dimensional RPs, GPU acceleration is advisable. For large data, it may be practical to save intermediate results from smaller grids and compute the nRL only for selected box sizes w.

3 Application to synthetic data

Synthetic data provides ideal conditions for highlighting certain properties of the nRL measure. The nRL is analyzed for the synthetic patterns in Figs. 1 and 2. For the periodic pattern without noise, the nRL has two distinct minima at $w = 25$ and $w = 44$ (Fig. 3 a). As mentioned above, minima represent length scales associated with evenly distributed recurrences and correspond to recurring sub-patterns in the image. At these length scales of the periodic pattern, the nRL values indicate that the RP (Fig. 1 b) is homogeneous at these scales. For this pattern, the characteristic length scales correspond to the wavelength of the periodic signal and its multiples.

The nRL curve of the periodic pattern with random white noise (Fig. 3 b) resembles the curve of the periodic pattern without noise, but the minima are less distinct. Adding noise yields a more realistic synthetic pattern while demonstrating that the underlying periodic pattern continues to shape the curve. The slight dip at the beginning of the curve originates from the increased homogeneity of the RP on small scales due to the fine-grained noise.

The nRL curve of the Sierpiński carpet exhibits distinct maxima (Fig. 3 c). They originate from the self-similar sub-patterns (especially the large squares measuring 3, 9 and 27 px) in the image, which form accumulations of recurrences in the RP, as well as larger gaps in the RP (Fig. 2 b), leading to a more heterogeneous distribution of recurrences across all evaluated scales.

Uniformly distributed white noise is a fine-grained pattern. This translates to the recurrences in the respective spatial RP (Fig. 2 d) and is reflected in a nRL curve that approaches a straight line without any extrema (Fig. 3 d). The fluctuations in the curve for larger box sizes originate from edge effects. While these fluctuations would disappear for an infinitely large white noise pattern, they are inevitable in practice due to the finite size of the image. To minimize these edge effects in real-world applications, the maximum box size for which the nRL is calculated must be carefully selected, taking into account the overall image extent.

Due to the limited spatial extent of the images and the minima and maxima, the underlying power law behavior is especially challenging to identify in the nRL curves of the periodic patterns (Fig. 3a and b) and the Sierpiński carpet (Fig. 3 c). Therefore, it is impossible to compare the steepness of the power law curves. Regarding the cut-off, it can be observed that while the nRL curve of the white noise pattern (Fig. 3 d) does not exhibit a cut-off, underlining the homogeneity of its RP on all scales, the curves of the periodic patterns and the Sierpiński carpet display later cut-offs. This relates to the fact that for the RPs of these patterns, heterogeneity persists on larger scales. For the periodic patterns, this originates from the larger gaps in the RP, whereas for the Sierpiński carpet,

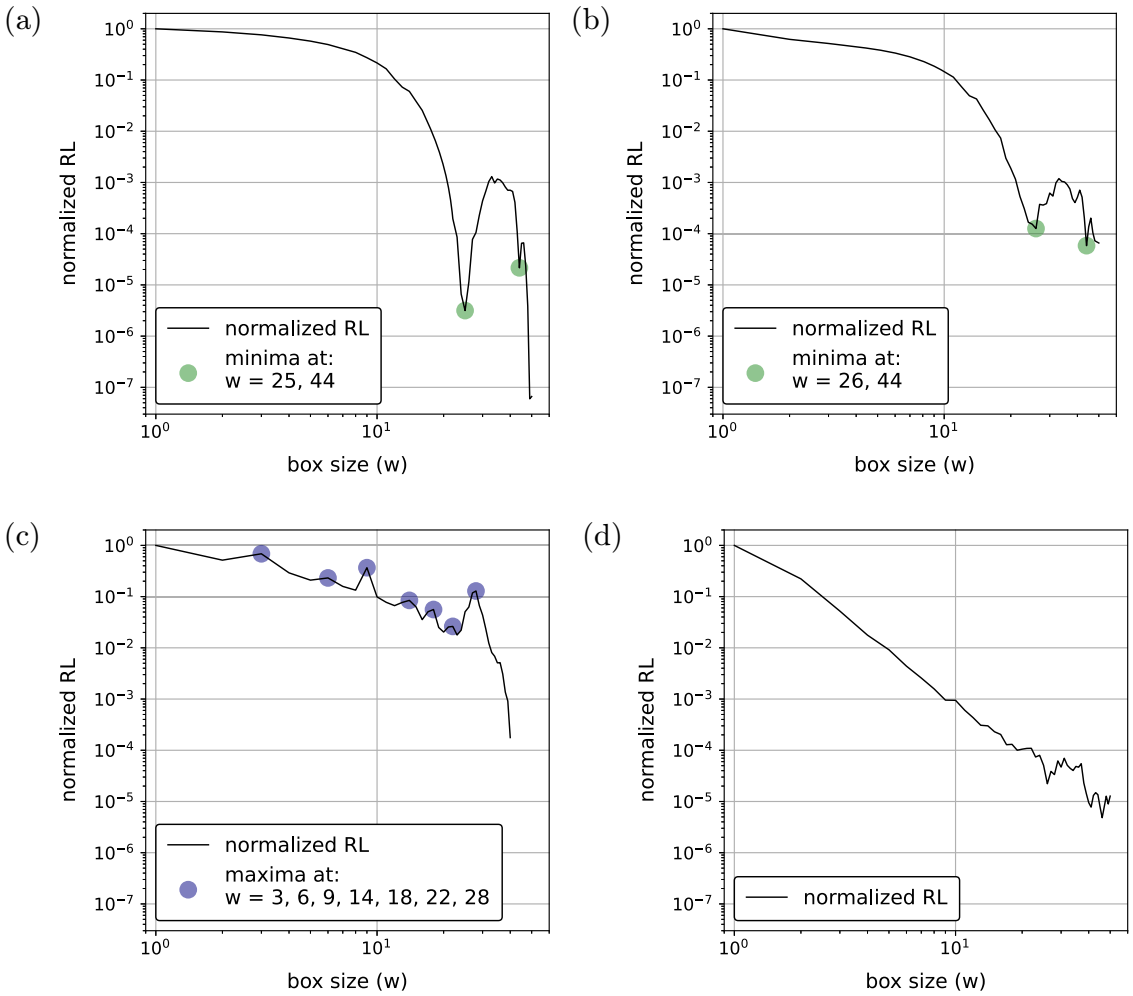

Fig. 3 Normalized recurrence lacunarity curves of the RPs of **a** the periodic pattern, **b** the periodic pattern with noise, **c** the Sierpiński carpet, **d** the uniformly distributed white noise that are displayed in Fig. 1 and Fig. 2

the high nRL values on smaller scales are related to accumulations of recurrences and gaps due to the extended self-similar sub-patterns in the underlying image.

The appearance of an RP depends heavily on the RR, which consequently influences the nRL. In this study, the RR is fixed at 20% for all patterns (except for discrete patterns). To evaluate the impact of the parameter, Appendix a provides a qualitative analysis of how different RRs influence the resulting nRL curves.

Taken together, the synthetic results validate how the nRL relates to the original data space: high nRL values relate to a heterogeneous RP characterized by accumulations of recurrences, which can originate from recurring sub-patterns with internal self-similarity (Sierpiński carpet) or gaps, which relate to outliers or spatial regime shifts in the data (not shown in this study). Low nRL values reflect a homogeneous RP, which can be linked to recurring sub-patterns (minima in the periodic patterns) or the systematic absence of recurring sub-patterns (uniformly distributed white noise).

4 Application to model data

To build a bridge between synthetic patterns and real-world data, the second data set investigated in this work consists of model data that finds application in the real-world context of biodiversity. The May-Leonard model (see Fig. Appendix B), introduced by [16], can be used to model competitive interactions between three species. [17] found the first biological example of such a system by observing a lizard population over several years.

The model is also referred to as a rock-paper-scissors (RPS) system, because it works in a non-hierarchical, cyclic way, just as the referenced game [17]. In the simulations, there are three species 1, 2, and 3 that interact

with each other based on the rules of the RPS system, e.g., 1 "defeats" 2, 2 "defeats" 3, and 3 "defeats" 1. In the simulations, each species can perform three actions: mobility (m), reproduction, and predation, each with an associated probability. The simulation starts with a random distribution of species and empty pixels in an N^2-sized grid. Using this model, [18] and [19] investigated the biodiversity depending on the mobility m. [18] found that for low mobility values, the biodiversity is preserved, the interactions happen locally, and a pattern of moving spirals is created. The more the mobility value increases, the larger the spirals get, until their wavelength is larger than the grid. Two snapshots from simulations with different m settings are displayed in Fig. 4 a and c, respectively. The original snapshots were smoothed using a median filter with a size of 10 px.

The smaller spirals of the $m = 0.2$ pattern lead to a more fine-grained RP (Fig. 4 b) compared to the RP of the $m = 0.8$ pattern (Fig. 4 d), which exhibits a coarser structure. In the nRL curves of both patterns, this is reflected in an earlier cut-off in the curve for the $m = 0.2$ pattern in comparison to the $m = 0.8$ pattern, since for the former the masses become translationally invariant at smaller box sizes and the accelerated decrease of nRL values starts at smaller scales. Future research could build upon these findings by studying how the cut-off is related to the size of the spirals and the underlying system parameters. After the cut-off, both curves exhibit a similar slope, originating from the fact that both patterns stem from the same system. The lack of minima and maxima indicates that the nRL does not detect any characteristic length scales within the system.

5 Application to coastal river catchments

To demonstrate the practical utility of the nRL measure in real-world applications, this section applies it to the hillslope gradients of 47 small coastal river catchments along the coast of California in the western United States of America (Fig. 5).

In the north of the area of interest lies the Mendocino Triple Junction (MTJ), which is the intersection of three tectonic plates: the Juan de Fuca Plate, the Pacific Plate, and the North American Plate [20–22]. The intersection of tectonic plates at the MTJ is associated with a migrating uplift wave, which propagates northward at a velocity of approximately 50 mm/yr [22, 23]. Catchments located south of the current uplift front have largely adjusted to the temporarily increased uplift rates, whereas catchments in the north are still in an early stage of response [22, 24].

An increase in uplift rate does not lead to an instantaneous and spatially uniform increase in hillslope gradients. Instead, uplift induces localized steepening, often expressed through the upstream migration of knickpoints and associated changes in channel incision. Hillslope adjustment follows with a delay and occurs heterogeneously across the landscape [25]. While overall slope angles are expected to stabilize at a certain value—[26] found this value to be approximately 15—20° for larger river catchments further inland in the same region—any additional uplift is expected to be compensated for through increased earthflow and landslide activity [26]. As a result, catchments affected by the uplift wave are expected to exhibit a spatial coexistence of two geomorphic equilibrium states, with some areas already adjusted to the new boundary conditions and others still reflecting pre-uplift topography. During this transient adjustment phase, the spatial structure of hillslope gradients is, therefore, expected to be less stationary than in catchments that have reached a long-term equilibrium. Rather than reflecting stochastic or chaotic dynamics, this structure arises from the superposition of different stages of landscape response. Evaluating changes in the spatial organization of hillslope gradients in relation to uplift rate thus provides complementary information to existing analyses based on channel steepness, as in [22], or distributional statistics, such as the upper percentiles of slope values as in [24].

The digital terrain models (DTMs; i.e., observational representations of the Earth's surface derived from topographic measurements, not to be confused with the computational model data of Sect. 4) as well as the derived hillslope gradients and the respective uplift rates were provided by [24]. Missing uplift rates were linearly interpolated. Due to computational limitations, only a central square within the river catchments with a maximum size of 1023 px × 1023 px was evaluated. The resolution of the DTM was downsampled to 4 m × 4 m using the local mean. Exemplary catchments are displayed in Appendix A.

The advantage of applying the nRL measure to the river catchments stems from the fact that the intermediate transformation into an RP offers a standardized way to convert the continuous data into a binary pattern. During this process, not only are all states of the image compared to each other (unlike for a simple threshold), but the data gets reduced to the information about spatial recurrences, and outliers are ignored (as long as they do not recur).

The nRL curves of all river catchments approach straight lines (Fig. 6; a visualization of the individual curves can be found in Appendix D), although they vary in steepness. This indicates differences in the homogeneity of the respective RPs. For steeper curves, the homogeneity of the underlying RP increases faster when moving to larger scales. In the context of the hillslope gradients, this means that there are fewer, smaller, or no recurring sub-patterns (which would lead to accumulations of recurrences), or regions of outliers or different spatial regimes (which would lead to gaps in the RP) in the data, leading to a fine-grained, seemingly more random distribution

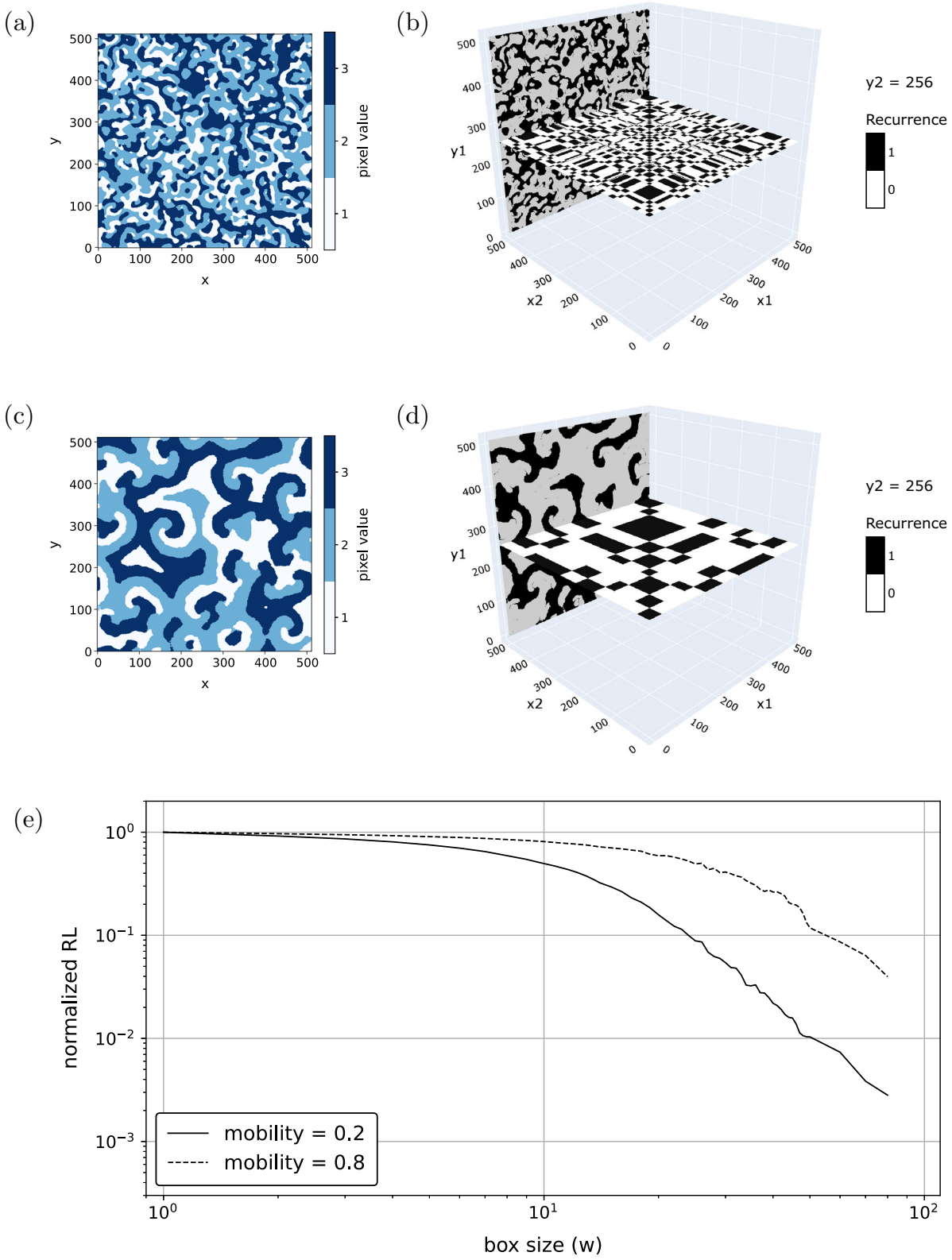

Fig. 4 Snapshots from RPS system simulations with their respective RPs and nRL curves. **a**, **b** simulation with $m = 0.2$, $\varepsilon = 0$; **c**, **d** simulation with $m = 0.8$, $\varepsilon = 0$; **e** the nRL curves of both patterns

of recurrences within the recurrence plot. This indicates that the hillslope gradient values in the underlying data exhibit a finer-grained and more irregular structure. This is consistent with catchments that are currently in a transient state of landscape adjustment, where characteristics of two different geomorphic equilibrium states coexist. A flatter curve would be expected for the catchments that have just started to adjust to the increase in elevation or are already in a new equilibrium state, since for these catchments, a more regular structure in the hillslope gradient values and, therefore, more (self-similar) recurring sub-patterns and larger accumulations of recurrences in the RP are expected, which lead to a consistently larger heterogeneity of the RP across scales. Furthermore, the nRL curves do not exhibit distinct minima or maxima, which indicates the lack of characteristic length scales within the data.

To gain further insights, a specific length scale, $w = 10$ (40 m, white dashed line in upper panel of Fig. 6) was chosen as an indicator of the relative positions of the curves, which is large enough to avoid the influence of noise, but small enough to not be affected by fluctuations for large box sizes that could relate to edge effects. The full nRL curves provide a complete picture of scale-dependent heterogeneity for the RP of each catchment, while the value at $w = 10$ serves as a consistent summary statistic for cross-catchment comparison, complementing the curve-based analysis. These scale-specific values of nRL are compared to the uplift rate of the corresponding catchment (lower panel of Fig. 6). Based on this comparison, a delayed response of the river catchments to the uplift rate can be assumed. A lower nRL value at $w = 10$ corresponds to a steeper and more linear decrease of the nRL curve, indicating that the corresponding RPs become homogeneous already at relatively small spatial scales (below 40 m), suggesting that the slope values follow a more fine-grained and random distribution. As explained above, such a pattern is expected during transient landscape adjustment, where regions influenced by recent uplift coexist with areas that have not yet responded. Higher nRL values at this scale indicate increased heterogeneity in the recurrence structure, which, given the validated relationship between recurrence structure and physical heterogeneity, is consistent with a landscape that is dominated by a single geomorphic state. The observed variability among catchments, therefore, supports the interpretation of a delayed response of hillslope gradients to tectonic forcing. The six catchments in the south (1 to 6) and the four catchments in the north (44 to 47) do not fit into this trend and suggest that other factors could influence homogeneity in the spatial distribution of the hillslope gradient values. One potential source of variability among these catchments is heterogeneity in the lithology, which is apparent in the geologic mapping of [27]. The fact that such assumptions can be derived from the nRL values underlines the various applications of the nRL measure.

6 Discussion

In the course of developing the method, several advantages of creating a spatial RP became evident: (1) The spatial RP includes additional information on directional changes within the image and, therefore, adds valuable information to the analysis of the spatial structure, and (2) the conversion of continuous data of different shapes to comparable binary patterns, which was underlined by the application to different data sets in this work. Moreover, a further benefit of combining the lacunarity with the spatial RPs is that it generalizes to multivariate or multi-channel spatial data.

Synthetic patterns were used to investigate the characteristics of the behavior, with a focus on the characteristic length scales revealed by minima and maxima in the nRL curves. Nevertheless, a wider range of synthetic data would better highlight the properties of the measure.

Whereas the synthetic patterns focused on the characteristic length scales, model data from an RPS system highlighted the power law behavior and especially the role of the cut-off (if present). More simulations could be used to investigate the significance of the results. Further, a quantitative study of the power law parameters could give valuable insights.

Using spatial RPs and their nRL, the spatial structure of hillslope gradients of 47 small coastal river catchments could be quantified and evaluated in a comparable way, while revealing differences among the catchments. Even though the method was able to detect differences among catchments that seem to be related to variations in the uplift rate, further assessment of the significance, as well as studies of the influence of other factors, are necessary. This includes a refinement of the uplift rates, which were previously only linearly interpolated, as well as the testing of additional resolutions of the DTMs and improved quality of the DTMs.

From a methodological perspective, several questions remain open for future research. First, the influence of the parameters used for the creation of the RPs, especially the RR, should be studied further. Since lacunarity is sensitive to point density, which is directly controlled by RR, a systematic sensitivity analysis of its influence on the nRL curves (in addition to Appendix A) is necessary to fully establish the robustness of the results. Although RR was fixed across all data sets to ensure comparability – consistent with standard practice in recurrence analysis [13] – the quantitative influence of this choice on the nRL values and their interpretation remains an important open question. It is, therefore, also important to note that the interpretation of nRL values as indicators of physical heterogeneity, while demonstrated for the synthetic and modelled test patterns studied here, may require

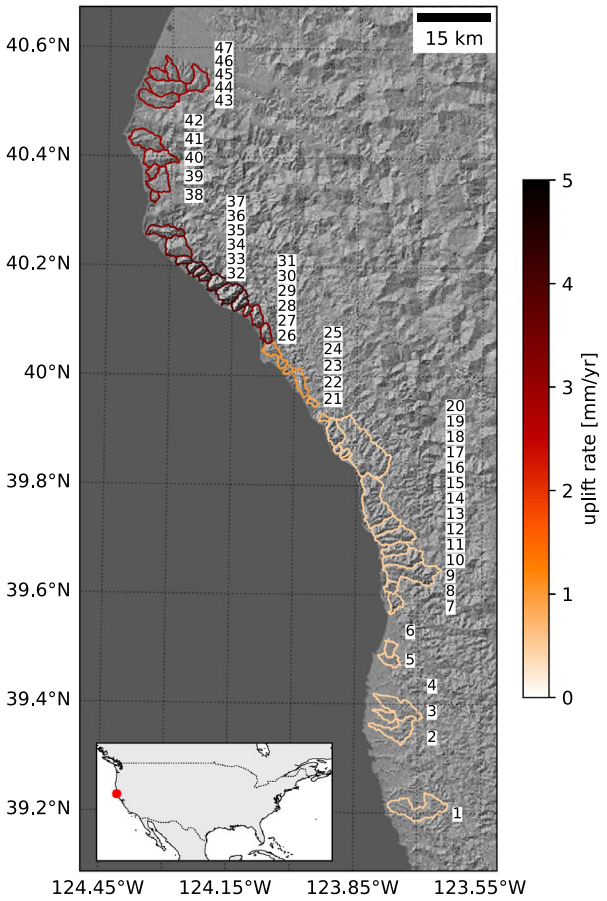

Fig. 5 Outlines of the 47 coastal river catchments along the northern California coast near the Mendocino Triple Junction (MTJ), colored by their associated tectonic uplift rates. The northward-migrating uplift wave results in systematically higher uplift rates in the northern catchments, whereas southern catchments have largely experienced earlier uplift and subsequent landscape adjustment. Catchment numbers correspond to those used in Fig. 6

re-validation for parameter ranges substantially different from those applied. The nRL should thus be understood as a measure of heterogeneity in recurrence structure that reliably reflects the spatial organization of the original spatial data under validated conditions, with the caveat that the sensitivity of this relationship to parameter choices, particularly RR, remains to be systematically quantified.

Second, the preprocessing of the data could influence the results. In addition, alternative grid definitions could be explored, such as shifted or overlapping boxes, or random box sampling, though random box sampling compromises reproducibility and all alternatives remain difficult to integrate with the current implementation.

Furthermore, if the characteristic length scales in the RP are of interest, a formal statistical criterion for the identification of significant minima and maxima in the nRL curve – for example through surrogate-based confidence intervals – would replace the visual classification and improve the general applicability of the method.

Finally, it is important to note that a significance assessment was not done in this work due to computational limitations. To be able to do a significance assessment or to process images larger than 1023 px × 1023 px, the computational approach needs to be refined, for example, by utilizing multiple or more powerful GPUs or a more efficient implementation of the algorithm. These represent important directions for future research.

7 Conclusion

In this paper, the concept of recurrence lacunarity (RL) was extended to spatial data, then validated by applying it to synthetic patterns and model data, and finally, its utility was demonstrated by evaluating the hillslope gradients of river catchments. The results showed that the nRL measure is able to detect differences in the spatial structure of hillslope gradients among the catchments, which were linked to local uplift rates as an external (environmental) influence. The hillslope gradients exhibit a finer-grained and more irregular structure for catchments that are expected to be in a transition between two geomorphic equilibrium states after the uplift wave. This is associated with a more homogeneous RP across all scales, which is effectively captured by the nRL.

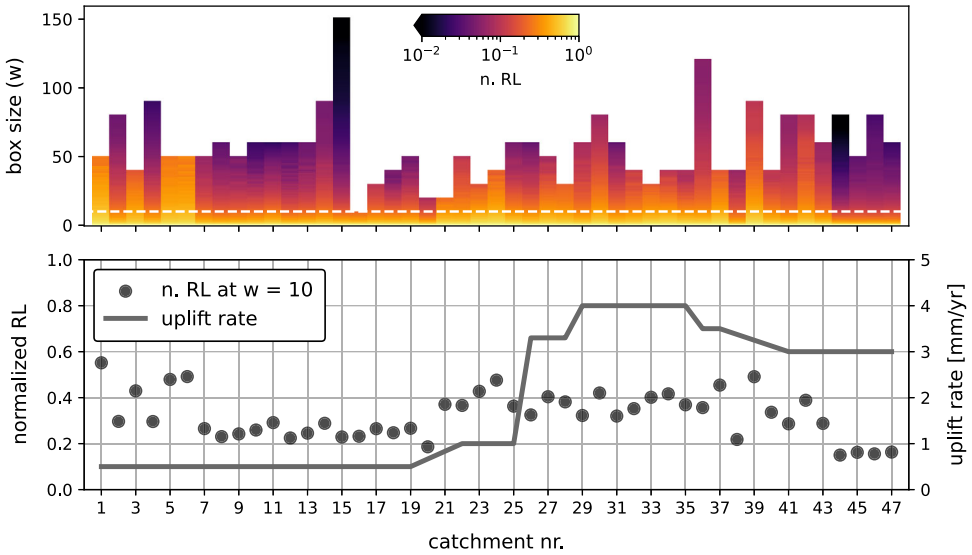

Fig. 6 Upper panel: Normalized recurrence lacunarity (nRL) curves of the hillslope gradient fields for all 47 river catchments (for the individual nRL curves in standard representation, see Fig. 10). Starting from a box size of $w = 50$, only every 10th nRL value was calculated. All curves approach a similar asymptotic behavior at large box sizes, whereas exhibiting systematic differences at intermediate scales. These differences reflect variations in the spatial organization of hillslope gradients, with some catchments showing earlier convergence towards homogeneity and others maintaining heterogeneity across a wider range of scales. The dashed line marks the selected reference scale $w = 10$ (corresponding to 40 m), chosen to balance sensitivity to spatial structure against noise and edge effects; Lower panel: Normalized recurrence lacunarity values at $w = 10$ (40 m) for all river catchments (black markers), shown together with the corresponding tectonic uplift rates (grey line). Lower nRL values indicate a more homogeneous recurrence structure at this scale, interpreted as the coexistence of hillslope regions at different stages of adjustment to tectonic uplift. Higher nRL values reflect increased spatial heterogeneity of the recurrences, consistent with catchments dominated by a single geomorphic state. The lack of a simple monotonic relationship highlights the delayed and spatially heterogeneous response of hillslope gradients to the migrating uplift wave, as well as the potential influence of additional factors, such as lithology

The nRL complements established statistical measures by capturing the spatial distribution of the data values. It can detect and quantify the relationship between (environmental) influences or model parameters and the spatial organization of data values. Beyond its demonstrated utility in remote sensing and geosciences, the measure is highly adaptable across several scientific domains. It has applications in image analysis in a medical context, is useful for damage detection, and can analyze surface structure in material science. Furthermore, the measure has potential in classification tasks and as features in machine learning applications.

Acknowledgements T. Braun acknowledges funding from the European Space Agency (ESA) Living Planet Fellowship through the *ARNETLAB* project [4000144018/24/I-DT-lr]. M. S. Palmero acknowledges the São Paulo Research Foundation (FAPESP) grants 2023/07704-5 and 2024/22136-6.

Funding Open Access funding enabled and organized by Projekt DEAL.

Data Availability The data for the synthetic patterns and the RPS system are included in the repository (link below). The data of the river catchments is published at https://doi.org/10.5281/zenodo.18454918.

Code availability The Python code to reproduce the results from this study is published at https://doi.org/10.5281/zenodo.18455017. The original implementation of recurrence lacunarity [4] is documented at https://github.com/ToBraun/RECLAC.

Declarations

Conflict of interest The authors declare that they have no conflict of interest.

Open Access This article is licensed under a Creative Commons Attribution 4.0 International License, which permits use, sharing, adaptation, distribution and reproduction in any medium or format, as long as you give appropriate credit to the original author(s) and the source, provide a link to the Creative Commons licence, and indicate if changes were made. The images or other third party material in this article are included in the article's Creative Commons licence, unless

indicated otherwise in a credit line to the material. If material is not included in the article's Creative Commons licence and your intended use is not permitted by statutory regulation or exceeds the permitted use, you will need to obtain permission directly from the copyright holder. To view a copy of this licence, visit http://creativecommons.org/licenses/by/4.0/.

Appendix A Sensitivity of normalized recurrence lacunarity to recurrence rate

See Appendix Fig. 7

Figure 7 displays the normalized recurrence lacunarity (nRL) curves of recurrence plots (RPs) generated from the synthetic test patterns (see Figs. 1 and 2) using different recurrence rates (RRs). As the RR increases, the nRL values consistently rise across all scales. This is related to larger accumulations of recurrences in RPs with higher RRs, which are a consequence of the increased recurrence threshold. For the periodic patterns, while the magnitudes of the extrema within the curves change depending on the RR, the core structural features of the curves remain well-preserved. These results demonstrate that the RR of 20% chosen for the analysis of the synthetic test patterns in this study is sufficient to accurately represent the characteristics of the nRL curves of the patterns. Furthermore, it validates the comparison of nRL curves across different patterns, provided the RR remains constant for all patterns. Note that the nRL curve of the Sierpiński carpet is excluded from this evaluation. As a discrete pattern, its recurrence threshold is fixed at $\epsilon = 0$, meaning its RR cannot be varied.

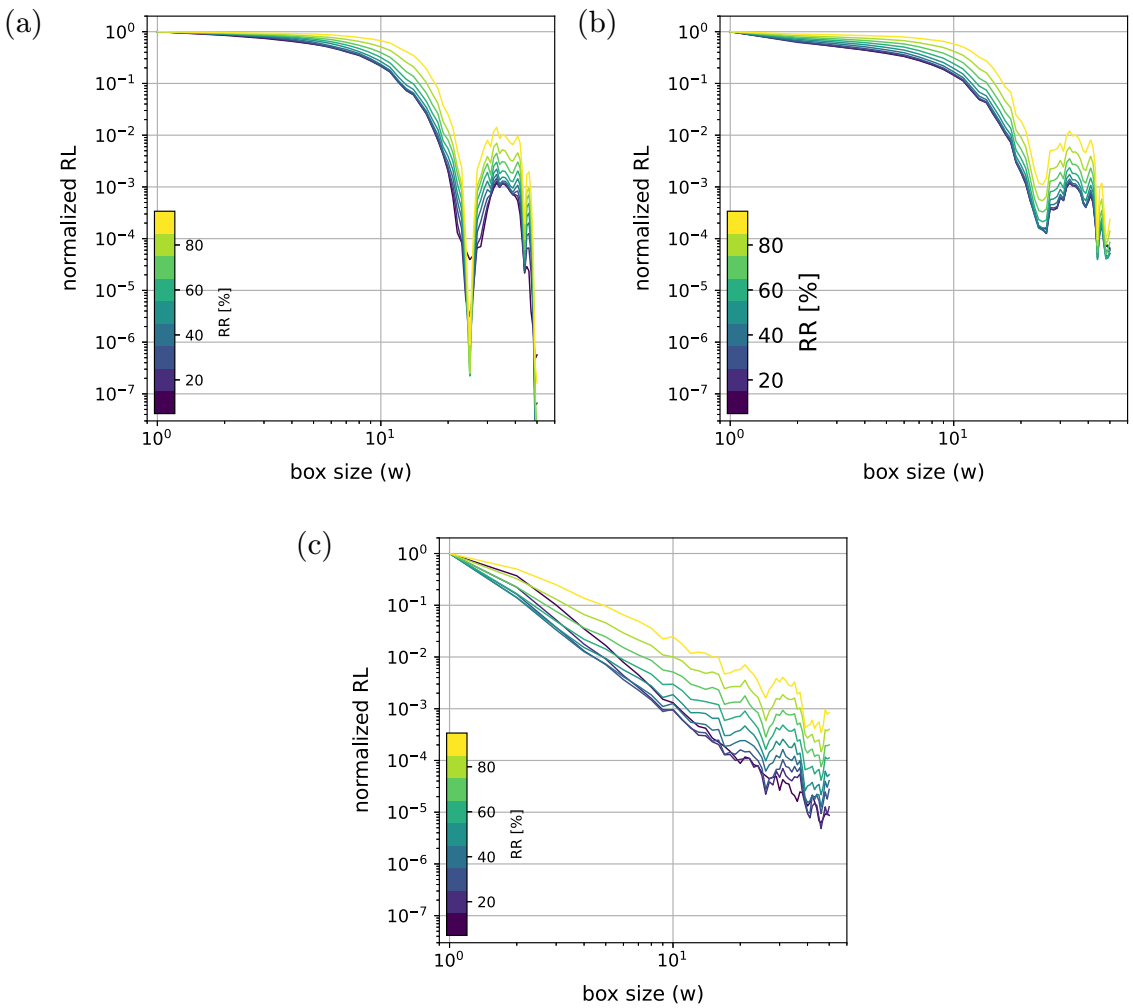

Fig. 7 Normalized recurrence lacunarity curves of the RPs with different recurrence rates (RRs) of **a** the periodic pattern, **b** the periodic pattern with noise, **c** the uniformly distributed white noise that are displayed in Fig. 1 and Fig. 2, respectively

Appendix B May-Leonard model

The May–Leonard (ML) model (also referred to as the rock–paper–scissors model, RPS) describes cyclic, non-hierarchical competition among three species (1, 2, 3) leading to dynamical coexistence. The population dynamics take place on a regular square lattice of size $N \times N$. The cyclical dominance follows the rules:

$$1 \to 2, \quad 2 \to 3, \quad 3 \to 1.$$

At the individual level, participants of each species are allowed to interact within their first neighborhood (up, down, left, and right) via three distinct actions: *mobility* (m), *reproduction* (r), and *competition* (c). The sum of these probabilities is conserved ($m + r + c = 1$). Without loss of generality, the number of free variables is often reduced by setting $r = c = (1 - m)/2$.

For the initial condition, a homogeneous state is prepared by randomly spreading individuals of species 1, 2, and 3, as well as empty spaces (represented by 0), throughout the N^2 sites. The system then evolves in time through Monte Carlo steps. At each step:

1. A random site i is chosen as the active site (an empty site can never be active).
2. A site j among its neighbors is randomly selected as the passive site.
3. One of the three actions is randomly selected based on its associated probability (m, r, c):
   - *Mobility (m):* The positions of the active and passive sites are swapped, $(i, j) \to (j, i)$, independent of the occupation in the passive site.
   - *Reproduction (r):* If the passive site is empty, it will be filled with one individual of the active species, $(i, 0) \to (i, i)$.
   - *Competition (c):* If the active and passive individuals satisfy the RPS dominance rule ($i \to j$), the passive individual is removed, creating an empty site, $(i, j) \to (i, 0)$.

Because this is an individual-based model, a generation is recorded after N^2 successful interactions between a random active site i and a passive neighbor j throughout the lattice.

To construct the images analyzed via recurrence lacunarity, the simulations are evolved over a predefined number of generations (e.g., $T = 5,000$) to bypass the initial transient phase. Once the system reaches its relaxed state, characterized by the emergence of spatial spiral patterns sustained by the mobility parameter, a 2D snapshot of the lattice is captured. This final state snapshot maps the spatial distribution and abundance of the species into a static image, which is then converted into a spatial recurrence plot.

Appendix C Exemplary river catchments

See Appendix Figs. 8 and 9.

To gain a better understanding of the evaluated hillslope gradient data, Figs. 8 and 9 display the river catchment nr. 5 and nr. 45 together with their RPs, respectively. The catchments are similar in size, which reduces potential methodological differences among the catchments. According to Fig. 6, catchment nr. 45 exhibits a steeper nRL curve than catchment nr. 5. This is also reflected in the structure of their respective RPs and indicates that the underlying hillslope gradient values have a more irregular structure for catchment nr. 45 than for catchment nr. 5. This can be visually confirmed by comparing the slope maps of both catchments. Even though the spatial structure of the hillslope gradients for both catchments seems not to be related to the uplift wave, they exhibit exceptionally regular or irregular structures of hillslope gradients compared to the other catchments, respectively.

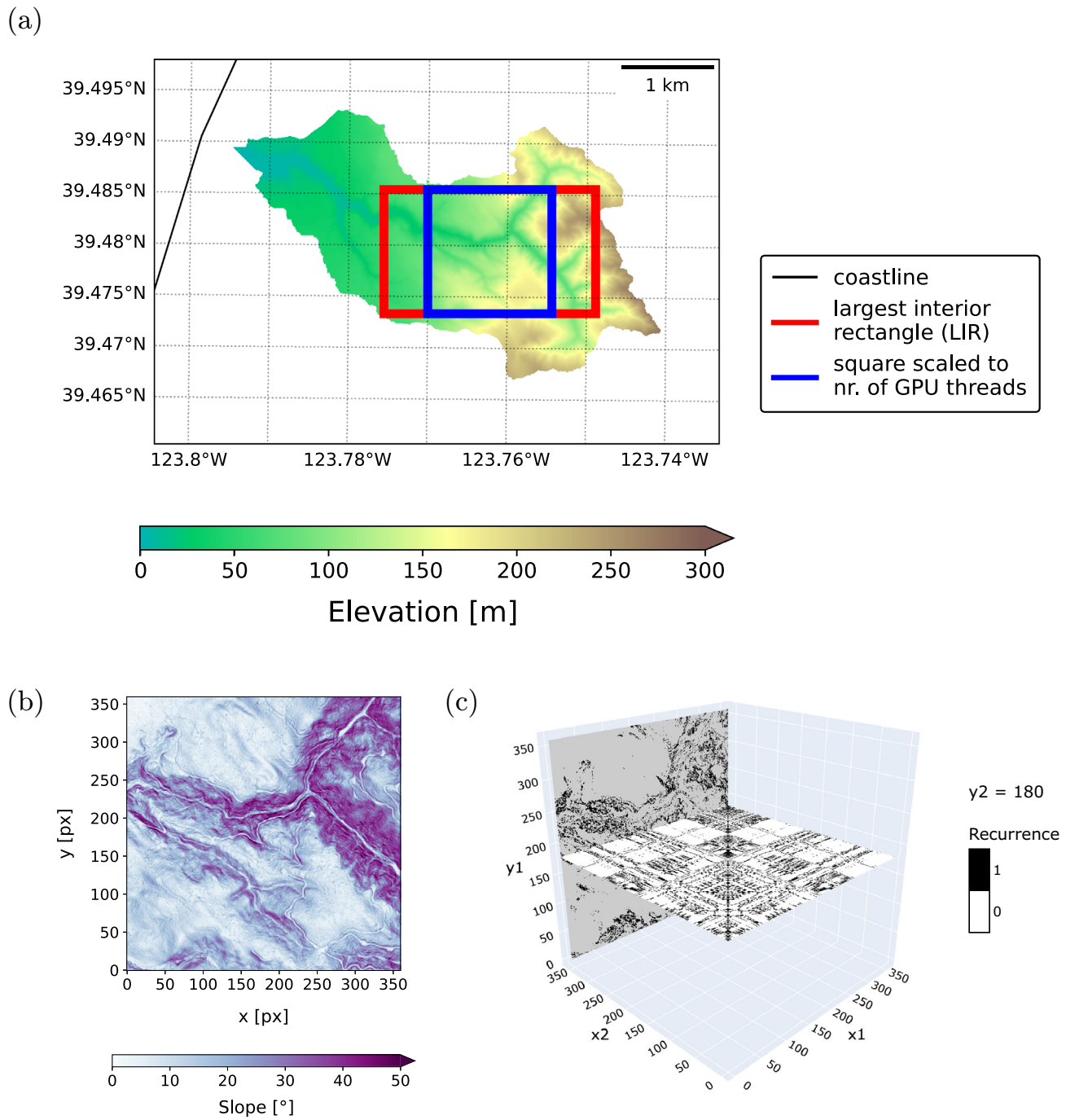

Fig. 8 Catchment nr. 5. **a** Displays the digital terrain model (DTM) together with the outline of the largest interior rectangle of the catchment (algorithm from [28]) and the outline of the square that is scaled to the number of GPU threads and was finally used for the analyses, **b** the hillslope gradient values that were the subject of the study, **c** the RP of the hillslope gradients with a $RR \approx 20\%$

Appendix D Normalized recurrence lacunarity curves of the river catchments

See Appendix Fig. 10.

In addition to Fig. 6, Fig. 10 visualizes the nRL curves of the river catchments as lines, colored by their associated uplift rates. As before, it is obvious that all curves approach straight lines that exhibit no distinct minima or maxima. The curves differ in their slope.

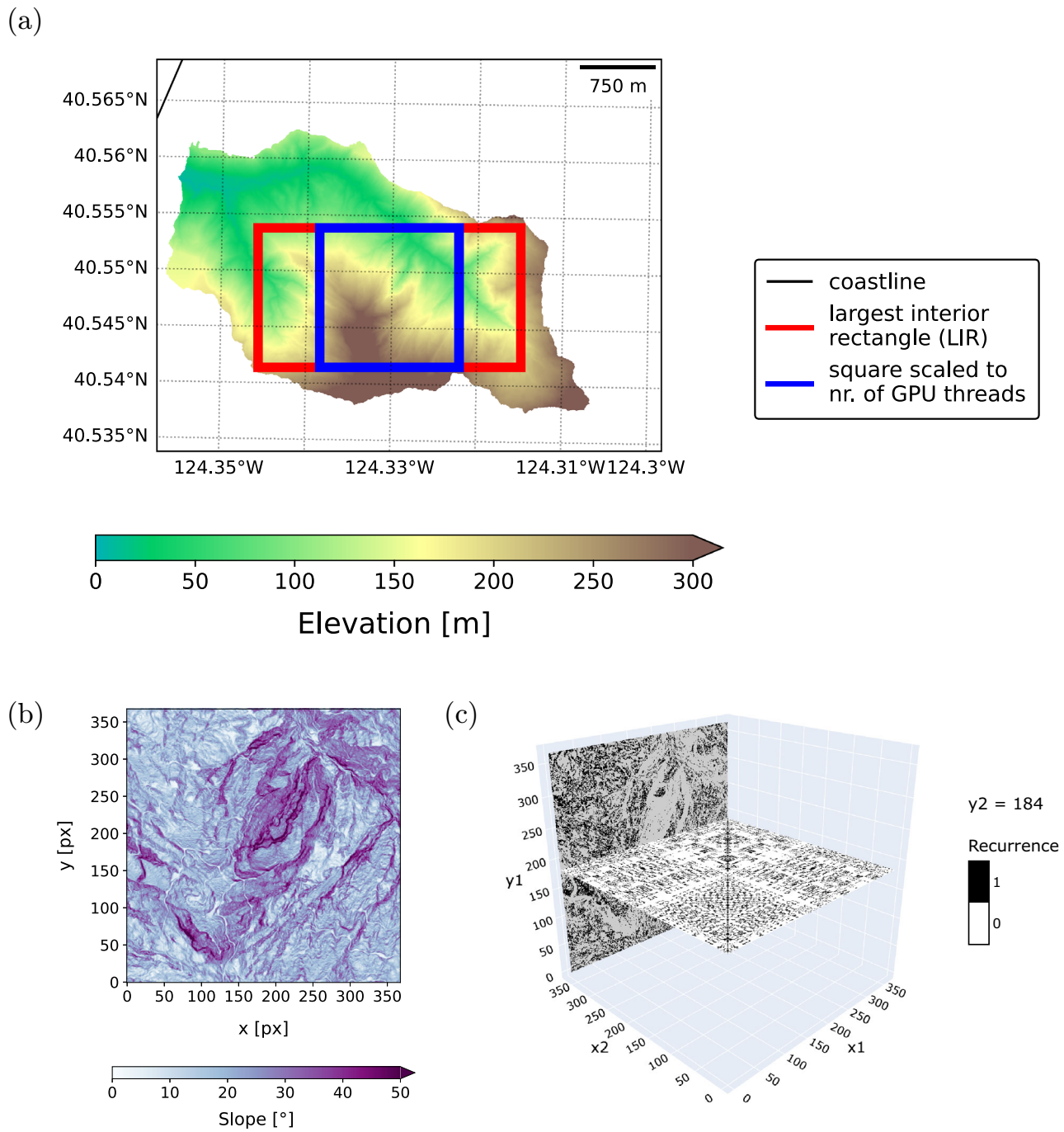

Fig. 9 Catchment nr. 45. **a** displays the digital terrain model (DTM) together with the outline of the largest interior rectangle of the catchment (algorithm from [28]) and the outline of the square that is scaled to the number of GPU threads and was finally used for the analyses, **b** the hillslope gradient values that were the subject of the study, **c** the RP of the hillslope gradients with a $RR \approx 20\%$

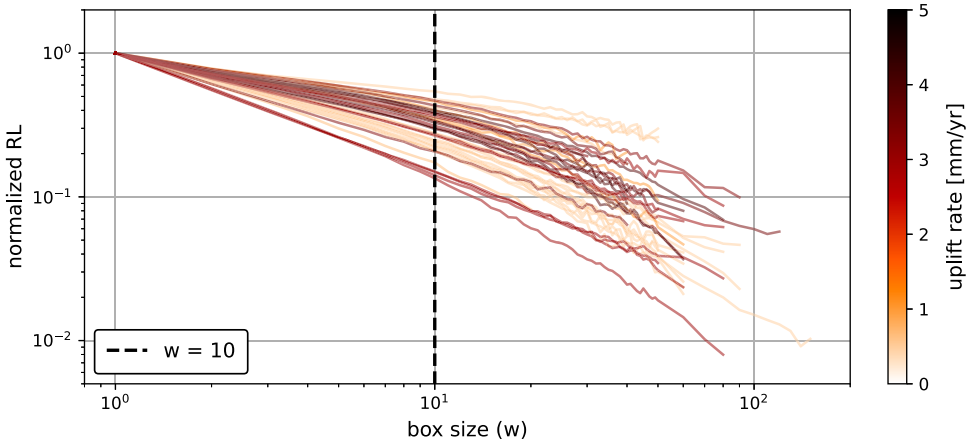

Fig. 10 Normalized recurrence lacunarity (nRL) curves of the hillslope gradient fields for all 47 river catchments. Starting from a box size of $w = 50$, only every 10th nRL value was calculated. Colors indicate the local uplift rate of each catchment. The dashed line marks the selected reference scale $w = 10$ (corresponding to 40 m). This standard representation complements Fig. 6, where the same curves are displayed in an alternative format to facilitate cross-catchment comparison

A relation between the shape of the curve and the uplift rate is not clearly visible. This is not surprising, since the river catchments are expected to respond to a change in the uplift rate with a delay. Furthermore, the curves do not exhibit distinct extrema, which means that there are no characteristic length scales in the data.

References

1. J.P. Eckmann, S.O. Kamphorst, D. Ruelle, Recurrence plots of dynamical systems. Europhys. Lett. (1987). https://doi.org/10.1209/0295-5075/4/9/004
2. J.P. Zbilut, C.L. Webber Jr., Embeddings and delays as derived from quantification of recurrence plots. Phys. Lett. A **171**, 199–203 (1992). https://doi.org/10.1016/0375-9601(92)90426-M
3. N. Marwan, N. Wessel, U. Meyerfeldt, A. Schirdewan, J. Kurths, Recurrence plot based measures of complexity and its application to heart rate variability data. Phys. Rev. E **66**(2), 026702 (2002). https://doi.org/10.1103/PhysRevE.66.026702
4. T. Braun, V.R. Unni, R.I. Sujith, J. Kurths, N. Marwan, Detection of dynamical regime transitions with lacunarity as a multiscale recurrence quantification measure. Nonlinear Dyn. **104**, 3955–3973 (2021). https://doi.org/10.1007/s11071-021-06457-5
5. B.B. Mandelbrot, *The Fractal Geometry of Nature* (W. H. Freeman & Co., San Francisco, 1983)
6. D. Mukhin, A. Hannachi, T. Braun, N. Marwan, Revealing recurrent regimes of mid-latitude atmospheric variability using novel machine learning method. Chaos **32**, 113105 (2022). https://doi.org/10.1063/5.0109889
7. R. Scott, H. Kadum, G. Salmaso, M. Calaf, R.B. Cal, A lacunarity-based index for spatial heterogeneity. Earth and Space Sci. (2022). https://doi.org/10.1029/2021EA002180
8. X. Mao, Z. Liu, J. Liu, W. Xie, P. Shang, Z. Shao, Measuring structural changes of recurrence patterns in multifractal and multiscale aspects by generalized recurrence lacunarity. Fractals **32**(1), 2450017 (2024). https://doi.org/10.1142/S0218348X24500178
9. A. Tomashin, G. Leonardi, S. Wallot, Four methods to distinguish between fractal dimensions in time series through recurrence quantification analysis. Entropy **24**, 1314 (2022). https://doi.org/10.3390/e24091314
10. N. Marwan, J. Kurths, P. Saparin, Generalised recurrence plot analysis for spatial data. Phys. Lett. A **360**, 545–551 (2007). https://doi.org/10.1016/j.physleta.2006.08.058
11. N. Marwan, M.C. Romano, M. Thiel, J. Kurths, Recurrence plots for the analysis of complex systems. Phys. Rep. **438**(5–6), 237–329 (2007). https://doi.org/10.1016/j.physrep.2006.11.001
12. F. Takens, Detecting strange attractors in turbulence. In: Rand, D., Young, L.-S. (eds.) Dynamical Systems and Turbulence, vol. 898, pp. 366–381. Springer, Coventry, England (1980). https://doi.org/10.1007/BFb0091924
13. K.H. Kraemer, R.V. Donner, J. Heitzig, N. Marwan, Recurrence threshold selection for obtaining robust recurrence characteristics in different embedding dimensions. Chaos **28**(8), 085720 (2018). https://doi.org/10.1063/1.5024914
14. G. Dougherty, G.M. Henebry, Fractal signature and lacunarity in the measurement of the texture of trabecular bone in clinical CT images. Med. Eng. Phys. **23**(6), 369–380 (2001). https://doi.org/10.1016/S1350-4533(01)00057-1
15. N. Marwan, P. Saparin, J. Kurths, Measures of complexity for 3D image analysis of trabecular bone. Euro. Phys. J. - Spec. Top. **143**(1), 109–116 (2007). https://doi.org/10.1140/epjst/e2007-00078-x

16. R.M. May, W.J. Leonard, Nonlinear aspects of competition between three species. SIAM J. Appl. Math. **29**, 243–253 (1975). https://doi.org/10.1137/0129022
17. B. Sinervo, C.M. Lively, The rock-paper-scissors game and the evolution of alternative male strategies. Nature **380**, 240–243 (1996). https://doi.org/10.1038/380240a0
18. T. Reichenbach, M. Mobilia, E. Frey, Mobility promotes and jeopardizes biodiversity in rock-paper-scissors games. Nature **448**, 1046–1049 (2007). https://doi.org/10.1038/nature06095
19. M.S. Palmero, M. Bongestab, N. Marwan, Investigating mobility in spatial biodiversity models through recurrence quantification analysis. arXiv (2025) https://doi.org/10.48550/arXiv.2507.18595
20. K.P. Furlong, R. Govers, Ephemeral crustal thickening at a triple junction:the mendocino crustal conveyor. Geology 27(2), (1999). https://doi.org/10.1130/0091-7613(1999)027<0127:ECTAAT%3e2.3.CO;2
21. J. Lock, H. Kelsey, K. Furlong, A. Woolace, Late neogene and quaternary landscape evolution of the northern california coast ranges: Evidence for mendocino triple junction tectonics. GSA Bull. **118**(9–10), 1232–1246 (2006). https://doi.org/10.1130/B25885.1
22. F.J. Clubb, S.M. Mudd, M.D. Hurst, S.W.D. Grieve, Differences in channel and hillslope geometry record a migrating uplift wave at the mendocino triple junction, California, USA. Geology **48**, 184–188 (2019). https://doi.org/10.1130/G46939.1
23. G.F. Sella, T.H. Dixon, A. Mao, Revel: a model for recent plate velocities from space geodesy. J. Geophys. Res. (2002). https://doi.org/10.1029/2000JB000033
24. A. Voigtländer, A. Rheinwalt, S. Tofelde, Quantifying earth's topography: steeper and larger than projected in digital terrain models. Geophys. Res. Lett. (2024). https://doi.org/10.1029/2024GL109517
25. E. Kirby, K.X. Whipple, Expression of active tectonics in erosional landscapes. J. Struct. Geol. **44**, 54–75 (2012). https://doi.org/10.1016/j.jsg.2012.07.009
26. G.L. Bennett, S.R. Miller, J.J. Roering, D.A. Schmidt, Landslides, threshold slopes, and the survival of relict terrain in the wake of the mendocino triple junction. Geology **44**(5), 363–366 (2016). https://doi.org/10.1130/G37530.1
27. C.W. Jennings, C. Gutierrez, W. Bryant, G. Saucedo, C. Wills, Geologic Map of California. https://ngmdb.usgs.gov/Prodesc/proddesc_96750.htm Accessed 2025-10-29
28. L.A. Weber, A.H. Zarei, Largest interior rectangle (2025). https://github.com/OpenStitching/lir/ Accessed 2025-07-25